In quest of cathode materials for Ca ion batteries: the $CaMO_3$ perovskites (M = Mo, Cr, Mn, Fe, Co, Ni)

M.E. Arroyo-de Dompablo[1,*], C. Krich[2], J. Nava-Avendaño[3], M.R. Palacín[3] and F. Bardé[2]

[1]Malta Consolider Team, Departamento de Química Inorgánica, Universidad Complutense de Madrid, 28040 Madrid, (Spain)

[2] Toyota Motor Europe, Research & Development 3, Advanced Technology 1, Technical Centre, Hoge Wei 33 B, B-1930 Zaventem, (Belgium).

[3] Institut de Ciència de Materials de Barcelona (ICMAB-CSIC) Campus UAB, E-08193 Bellaterra, Catalonia, (Spain)

*Corresponding author: e.arroyo@quim.ucm.es

Abstract

Basic electrochemical characteristics of $CaMO_3$ perovskites (M = Mo, Cr, Mn, Fe, Co, Ni) as cathode materials for Ca ion batteries are investigated using first principles calculations at the Density Functional Theory level (DFT). Calculations have been performed within the Generalized Gradient Approximation (GGA) and GGA+U methodologies, and considering cubic and orthorhombic perovskite structures for Ca_xMO_3 (x = 0, 0.25, 0.5, 0.75 and 1). The analysis of the calculated voltage-composition profile and volume variations identifies $CaMoO_3$ as the most promising perovskite compound. It combines good electronic conductivity, moderate crystal structure modifications, and activity in the 2-3 V region with several intermediate Ca_xMoO_3 phases. However, we found too large barriers for Ca diffusion (around 2 eV) which are inherent to the perovskite structure. The $CaMoO_3$ perovskite was synthetized, characterized and electrochemically tested, and results confirm the predicted trends.

Keywords: Perovskites, Ca-ion batteries, $CaMoO_3$, Ca insertion

Introduction

The development of rechargeable batteries based on the intercalation reaction of multivalent cations (Ca^{2+}, Mg^{2+}, Al^{3+}) is a current challenge for energy storage [1]. Designing such batteries demands the identification of competitive electrode materials and electrolytes for each particular active ion (Ca^{2+}, Mg^{2+}, Al^{3+}). A major advance in the Ca ion battery technology is the recently reported feasibility and

reversibility of calcium plating in conventional alkyl carbonate electrolytes at moderate temperatures [2]. At this very early stage of the Ca-ion technology, the quest for a high specific energy cathode material is an active field. While reports of reversible Ca insertion in V_2O_5 [3, 4], FeS_2 , Mo_3Se_4 [5], MFCN (Manganese HexaCyanoFerrate) exist [6] so far none of these materials exhibited large specific capacity nor good retention with cycling. The general goal of our work is the identification of alternative materials able to function as positive electrode in Ca ion batteries.

Computational techniques are a unique tool to quickly screen a variety of structures and compositions to identify potential electrode materials for these novel technologies. The capability of DFT to investigate Li intercalation electrode materials is well documented in several reviews [7-11]. The general strategy is firstly to calculate average voltage and volume changes associated to the Li insertion reaction. Further, DFT theory could be applied to gather additional information regarding electronic and ionic conductivities, crystal structure of intercalated phases and precise voltage-composition-curves at various temperatures. In short, the relevant electrochemical characteristics of a potential electrode material can be anticipated from DFT calculations. Recently a systematic computational screening has been applied to spinels AM_2O_4 as positive electrode materials for multivalent ion batteries [12]. This study revealed the virtual $[Ca]_T[Mn_2]_OO_4$ spinel as a promising cathode material for Ca ion batteries in terms of voltage, specific capacity and ionic diffusion.

Aiming to expand the map of possible electrode materials for Ca ion batteries we focus on another major structural family of oxides, the ABO_3 pervoskites. The skeleton of this structure is built up from corner-sharing MO_6 octahedra with the A cation in 8-fold coordinates sites. The A sites are too large to be fully occupied by the small Li cation (r_{VIII} = 0.92 Å [13]), reason why perovskites are discarded as high specific capacity electrode materials for Li ion batteries. On the contrary, a rich chemistry exists for perovskites with the larger Ca ions (r_{VIII} = 1.12 Å [14]) residing in the A sites, being the simplest composition $CaMO_3$. This family of compounds has been studied due to their interesting, albeit complex, electrical and magnetic properties. The perovskites under investigation in this work are $CaMO_3$ with M = Mo, Cr, Mn, Fe, Co, Ni. While the phases with M = Mo [15], Cr [16] , Mn [17] and Fe [18] are reported in the literature, to the best of our knowledge the compounds with M = Co and Ni have never been prepared. The maximum theoretical specific capacities of the different perovskites investigated in this study are given in Table I (in **SI**) as an indication. Assuming a 100% de-intercalation of calcium from $CaMO_3$, the theoretical capacities fall between 291 mAh/g (M = Mo) and 383 mAh/g (M = Cr).

We have performed a first principles investigation at the Density Functional Theory level (DFT), assuming that Ca ions can be deinserted from $CaMO_3$. For all the materials we have predicted the average voltage and volume changes for the full extraction of Ca ions, which would corresponds to the charge of the Ca//$CaMO_3$ battery. The full Ca removal from $CaMO_3$ requires the oxidation of M^{4+} to

the formal oxidation state M^{6+}. Since too high oxidation states are unlikely for Mn, Co, Fe and Ni we have also studied the possibility of partially deinserting Ca ions from $CaMO_3$ compounds (Ca_xMO_3). The constructed V-x profiles let us select $CaMoO_3$ as an interesting material for the further investigation of Ca mobility. Following this computational research, in this manuscript we report the synthesis, characterization and electrochemical testing of $CaMoO_3$ in three electrode Ca ion cells.

Methodology

Computational. The calculations have been performed using the ab-initio total-energy and molecular dynamics program VASP (Vienna ab-initio simulation program) developed at the Universität Wien [19]. Total energy calculations based on Density Functional Theory (DFT) were performed within the General Gradient Approximation (GGA), with the exchange and correlation functional form developed by Perdew, Burke, and Ernzerhof (PBE) [20]. The interaction of core electrons with the nuclei is described by the Projector Augmented Wave (PAW) method [21]. The energy cut off for the plane wave basis set was kept fix at a constant value of 600 eV throughout the calculations. The integration in the Brillouin zone is done on an appropriate set of *k*-points determined by the Monkhorts-Pack scheme. A convergence of the total energy close to 10 meV per formula unit is achieved with such parameters. The crystal structures of Ca_xMO_3 (x = 0, 0.25, 0.5, 0.75, 1) were fully relaxed (atomic positions, cell parameters and volume). Spin polarized calculations were performed in all cases. The final energies of the optimized geometries were recalculated to correct the changes in the basis set of wave functions during relaxation.

Orthorhombic perovskites $CaMO_3$ are known for Mo, Cr, Fe and Mn. Modelling their complex magnetic and electronic properties remains a challenge for first principles calculations [22-29]. Few DFT works have been reported for M = Cr, Mn and Fe. In some of these works the validity of GGA vs. GGA+U was discussed. From those investigations one can infer that the appropriate methodologies are: $CaCrO_3$ GGA or GGA+U with U below 1.5 eV [30], $CaMnO_3$ GGA+U with U 3-4 eV [25], and $CaFeO_3$ GGA+ U with large U values of 8 eV [31]. This evidences that a unique methodology can not be applied to systematically study the whole $CaMO_3$ family. Therefore, we have also calculated the total energies of the Ca_xMO_3 compounds using the GGA+U method, following the simplified rotationally invariant form of Dudarev, et al.[32]. Effective *U* values (J = 1 eV) for the *d* orbitals of M ions were set to 3 eV. For M = Co and Fe additional U_{eff} values of 4, 5 and 6 eV were used.

Calcium mobility in $CaMoO_3$ was investigated computationally using the Nuged Elastic Band method (NEB) as implemented in VASP. We considered $Ca_{15}Mo_{16}O_{48}$ and $Ca_{31}Mo_{32}O_{96}$ supercells where one Ca site is removed creating a vacancy. Constant volume calculations were performed for three

intermediate images. To calculate the energy at the saddle point, cubic splines were fit through the images along each hop.

Experimental. We followed the synthesis procedure described in [15]. $CaMoO_4$ is commercially available (Alfa Aesar Pro.Nr. 41865, 99.8%) and was thus used as a precursor. The reduction from Mo^{6+} to Mo^{4+} was achieved at high temperature under Ar/H_2−4% (commercial mixture) atmosphere. The temperature was increased at 300°C/h under air up to 1200°C. The moment this set point temperature of 1200°C is reached, the reducing gas flow is turned on by first purging and then reducing the flow to 60 l/h at 1.6 bar and kept for 4 hours. After the 4h reducing treatment at 1200°C, the cooling period is carried out under argon, with a small flow being kept until a temperature of 400°C is reached. From then on, without any gas flow, the oven is given time to cool down until the crucible is retrieved.

$CaMoO_3$ powder was ground and mixed with carbon black and binder (polyvinylidene fluoride, in short PVDF) in a weight ratio of 80:10:10. N-Methyl-2-pyrrolidone (NMP) was added to obtaina slurry which was further coated on an aluminium foil with a blade gap of 350 μm. Subsequently, the foil was dried in a vacuum oven at 80°C for 24 hours. Electrodes were punched from the coated foil (typical loading ca. 12 mg of active material) and tested in three electrode Swagelok cells using calcium discs as counter CE and reference RE electrodes [2]. The electrolyte used was 0.4M $Ca(BF_4)_2$ in EC:PC 1:1. The water content in the electrolyte was measuredd using a Karl Fischer technique and determined to be 110 ppm. Galvanostatic cycling with potential limitation (GCPL) at C/100 and potentiostatic intermittent titration technique (PITT, 5mV steps with duration limited by a C/200 current threshold) tests were conducted at 75°C and 50°C.

A Rigaku MiniFlexII X-Ray diffractometer was used for structural characterization of the as prepared powders and the electrodes both before and after cycling. A dome sample holder with a kapton foil window was used to prevent contact of samples with air. Rietveld refinements were performed using Fullprof program [33].

Results and Discussion

Calculations were performed within both the GGA and GGA+U. In order to have a general overview of the expected electrochemical properties, the results from both methodologies will be discussed in parallel. In addition, the total energies of $CaMO_3$ and MO_3 have been calculated using two crystal structures; the perfect cubic perovskite and the orthorhombic-distorted, which is the stable form reported for the known $CaMO_3$ compounds (M = Mo, Cr, Mn, and Fe). For all $CaMO_3$ both GGA and GGA+U predict that the orthorhombic form is more stable than the cubic one (see **figure 1** in S.I.).

Table 1 compares the calculated lattice parameters for the orthorhombic symmetry (GGA and GGA+U approximations) to the experimental ones. A good agreement is achieved, with errors below 3%. For the virtual MO_3 compounds the cubic symmetry is predicted as slightly more stable for M = Cr, Mo, as expected for their d^0 configuration in the formal oxidation state of M^{+6} (**figure 1** in S.I.). On the contrary, the orthorhombic symmetry is much more stable than the cubic for deinserted pervoskites containing Fe, Co and Ni (see S.I.). **Table II** in S.I. summarizes the calculated lattice parameters of the virtual MO_3 compounds.

TABLE 1. Calculated lattice parameters (in Å) for orthorhombic $CaMO_3$ structures (S.G. *Pnma*) within the GGA and the GGA+U method. Experimental values are also listed.

TM	Approximant	*a*	*b*	*c*
Mo	GGA	5.649	7.813	5.457
	GGA+U	5.753	7.833	5.502
	Experimental [15]	5.582	7.780	5.451
Cr	GGA	5.376	7.516	5.289
	GGA+U	5.459	7.519	5.311
	Experimental [34]	5.319	7.489	5.291
Mn	GGA	5.363	7.500	5.283
	GGA+U	5.386	7.540	5.312
	Experimental [17]	5.279	7.448	5.264
Fe	GGA	5.355	7.509	5.309
	GGA+U	5.407	7.585	5.350
	Experimental [18]	5.351	7.539	5.325
Co	GGA	5.329	7.434	5.276
	GGA+U	5.404	7.496	5.317
Ni	GGA	5.353	7.457	5.275
	GGA+U	5.342	7.439	5.260

For the large Ca^{2+} cation (r_{VIII} = 1.12 Å), a critical factor to screen is the volume variation of its crystal lattice upon calcium deintercalation. Excessive volume variations compromise the reversibility of the intercalation reaction and may induce instability of the deinserted materials versus amorphization or decomposition. Even if the reaction is reversible, long term cycling will be impeded if crystal structural modifications are relevant. **Figure 1** shows the calculated volume for orthorhombic $CaMO_3$ and MO_3 (GGA and GGA+U). For the pristine $CaMO_3$ materials, there is a good agreement between calculated and experimental volumes (differences below 5%). Compared to experimental values, the variations across the 3d series are better reproduced within the GGA+U than within the GGA. For the deinserted MO_3 (virtual compounds, never synthesized), the predicted GGA and GGA+U volumes are quite different for Fe and Co. This arises from a notorious difference in the predicted electronic and magnetic properties, which is out of the scope of this paper. Nevertheless, in all cases Ca extraction from $CaMO_3$ implies an important volume reduction. Calculated volume variations (($VCaMO_3$-

VMO_3)*100/$VCaMoO_3$) are of the order of 20% which is by far excessive for good electrode performance. In this sense, reversible full Ca deinsertion seems more favoured for Mo, with a calculated volume contraction of around 10%.

The ability to screening materials is limited by the voltage stability window of the electrolyte. The currently available non-aqueous Ca electrolytes can operate in a 1-4V potential window. The calculated average voltages for the full deinsertion reaction $CaMO_3$ → MO_3 + Ca are shown in **figure 2,** assuming cubic perovskites (black symbols) and orthorhombic structures (blue symbols). The crystal structure has a clear impact in the calculated voltage for Fe and Co. Regarding the two methodologies, GGA (circles) and GGA+U (squares), not surprisingly the calculated voltage within the GGA+U are higher, with the maximum difference being 0.5 V. Test for higher U values for Fe and Co (not shown for conciseness) barely vary the calculated voltage. Taking into account the effects of the crystal structure (cubic or orthorhombic) and computational approximation (GGA or GGA+U), the predicted average voltages for Cr, Mn, Fe, Co and Ni span in a voltage range 3.5-4.5 V. The Mo perovskite shows a calculated voltage of 2.1-2.7 V similar to the one reported for the Li insertion in MoO_3 (2.4 V) [35], which is reasonable since the same redox couple (Mo^{4+}/Mo^{6+}) is involved.

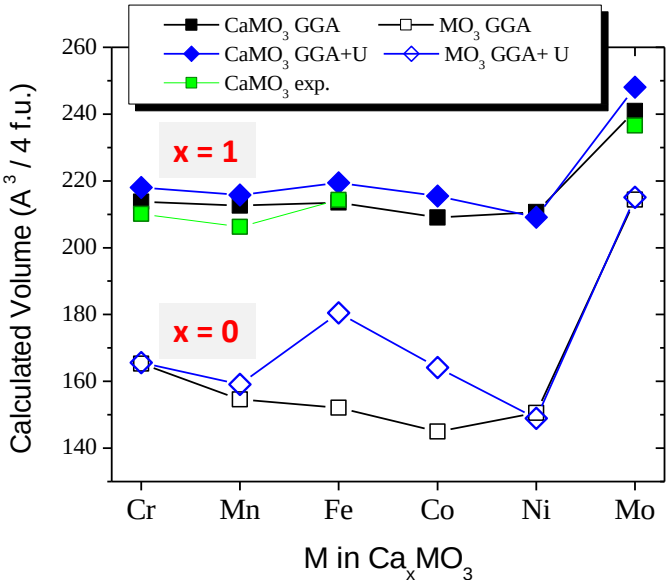

Figure 1.- Calculated volume for the unit cell of Ca_xMO_3 orthorhombic perovskites with x = 1 and 0. Experimental available values are plotted for comparison.

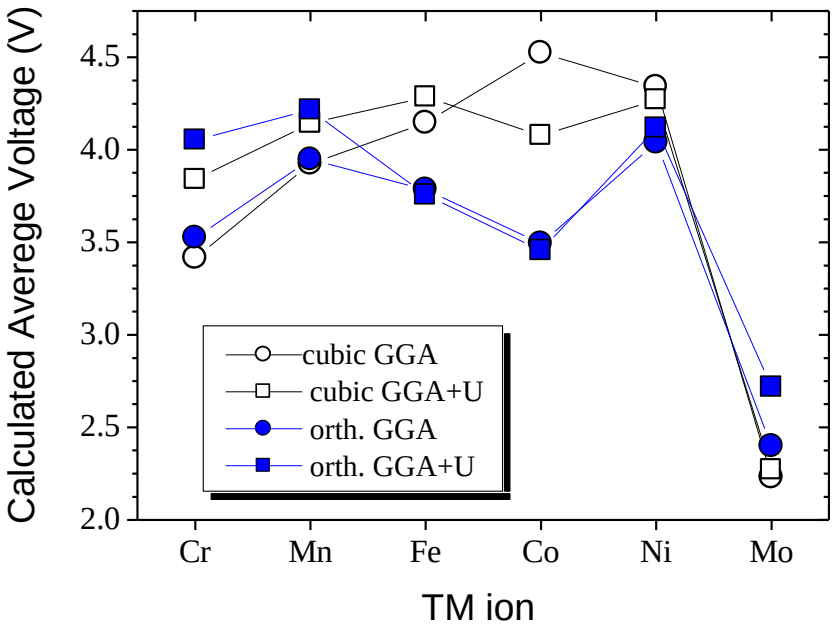

Figure 2.- Calculated average voltage for the reaction MO_3+ Ca → $CaMO_3$ within the GGA (circles) and the GGA+U (squares). Grey and blue colours denote orthorhombic and cubic symmetry, respectively.

So far, we have analysed the calculated average voltage and volume variations for the reaction MO_3 + Ca → $CaMO_3$. The results point at $CaMoO_3$ as the most interesting alternative, given the average voltage of c.a. 2.5 V and a volume variation of 10%. In terms of applications, none of the other perovskites will work efficiently at their maximum specific capacity. Yet it might be possible to *partially* deinsert Ca from them at a reachable voltage and with moderate crystal structure modifications. To investigate this possibility we have calculated the total energy of Ca_xMO_3 structures at x values of 0.25, 0.5 and 0.75. In this preliminary investigation we keep constrained to the unit cell of the perovskite ($Ca_4M_4O_{12}$), with only one possible Ca-vacancy arrangement at x=0.25 and 0.75, and three possible configurations at x = 0.5. We define the formation energy for a given Ca-vacancy distribution with composition x as:

$$\Delta_f E = E - x\, E_{CaMO3} - (1-x)\, E_{MO3} \qquad (1)$$

Where E is the total energy of the configuration per Ca_xMO_3 formula unit, E_{CaMO3} is the energy of the inserted perovskite and E_{MO3} is the energy of the deinserted perovskite. A negative formation energy $\Delta_f E$ indicates that the structure is stable with respect to phase separation into $CaMO_3$ and MO_3. The formation energies of Ca_xMO_3 allow us to determine the ground state energy *vs.* composition curve (convex hull), (see **figure 2** in S.I.). The convex hull has several vertices at which characteristic ordered structures of Ca ions and vacancies appear. These ground states result in single phase regions in the voltage composition curve at 0 K. We found that the formation energies for Fe, Co, Ni systems

are, generally speaking, positive within either the GGA or the GGA + U. The general trend for Cr and Mo is to have negative formation energies, meaning that single-phase regions would appear in the voltage-composition curve, i.e, partial deinsertion from $CaMoO_3$ and $CaCrO_3$ is feasible. For Mo, ground states appear at x = 0, 25, 0.5 and 0.75 (GGA). Ca_xMnO_3 is a complex system as GGA gives negative formation energies and GGA+U positive ones. Previous works indicate that the GGA+U approximation is more appropriate to reproduce the physical properties of this perovskite [23].

From the convex hull we can construct the voltage-composition profile for each $CaMO_3$ perovskite within the GGA and the GGA+U (**figure 3)**. The calculated volume variation between two consecutive single phases is given as a percentage. Generally speaking, the GGA and GGA+U give qualitatively very similar results, though the GGA+U predicts higher calculated voltages. $CaMoO_3$ displays a rich voltage-composition curve, due to the stability of intermediate Ca_xMoO_3 phases. The volume variation between two consecutive Ca_xMoO_3 intermediate phases is moderate. In addition, $CaMoO_3$ is a metallic compound [36], making this material an attractive potential electrode for Ca ion batteries. $CaCrO_3$ is another metallic compound [28], for which DFT predicts moderate deinsertion voltages. However, extraction of Ca to produce the stable intermediate $Ca_{0.25}CrO_3$ would induce a severe cell volume increase. The other TM-perovskites do suffer of important volume variations and/or present high operating voltages (above 3.5 V). $CaNiO_3$ might have some electrochemical interest, but its synthesis is not an easy task.

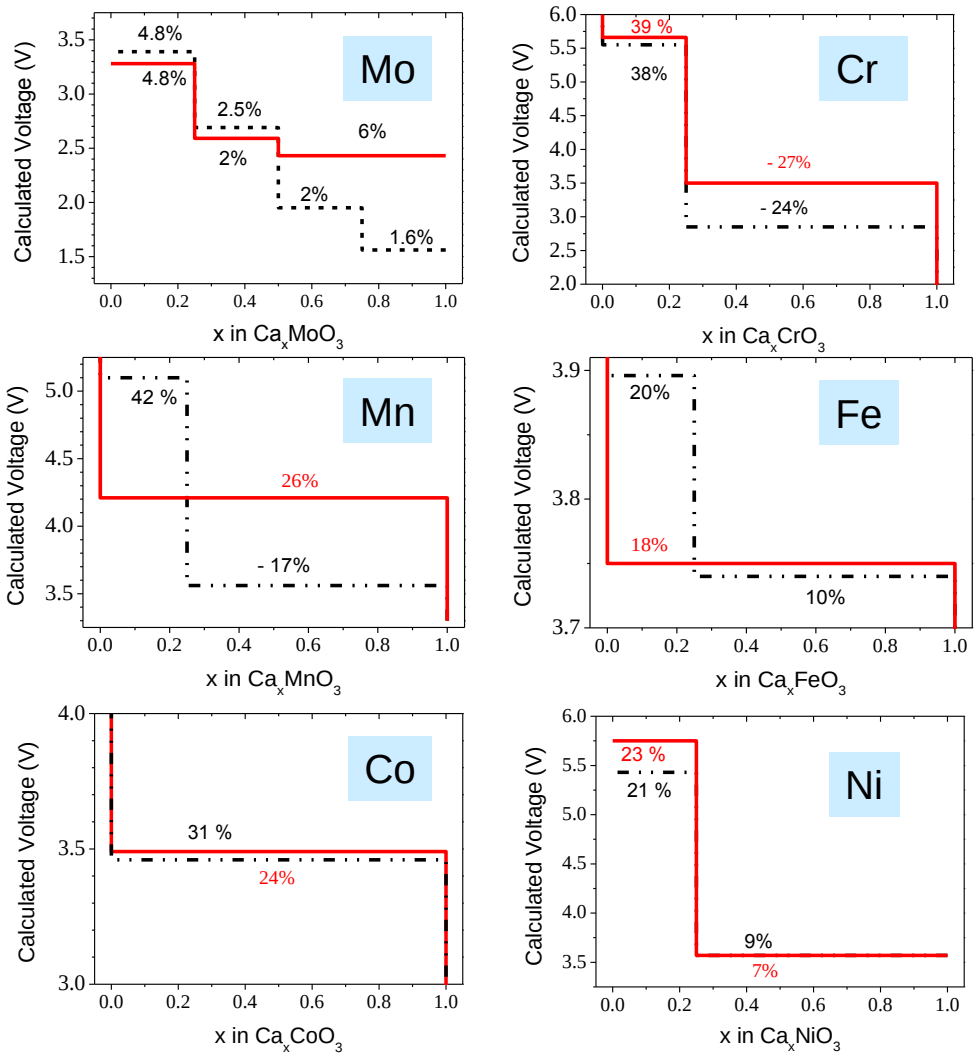

Figure 3.- Calculated sketch of the voltage – composition curve for Ca_xMO_3 perovskites. GGA in dashed black and GGA+U with U_{eff} = 3 eV in red. The volume variation between two consecutive single phases is given as percentage for the deinsertion process.

The preliminary screen points to $CaMoO_3$ as the most interesting among the studied $CaMO_3$ perovskites. It combines good electronic conductivity, moderate crystal structure modifications, activity in the 2-3 V region, and several intermediate Ca_xMoO_3 stable phases. Yet the mobility of Ca ions in this structure might be a limiting point. We have investigated the mobility of Ca ions in the perovskite $CaMoO_3$ constructing $Ca_{15}Mo_{16}O_{48}$ supercells with a = 11.2 Å, b= 7.8 Å and c= 10.9 Å, where the distance between the defects (vacant Ca sites) is of 7.8 Å. Due to the orthorhombic symmetry, two possible paths have been analysed (see **figure 4**). The first path connects Ca sites that are 3.95 Å apart along the y-axis while in the second path the distance is of 3.8 Å in the xz plane. The initial and final Ca sites share edges, being connected through a site labelled with a red cross in **figure 4b**.

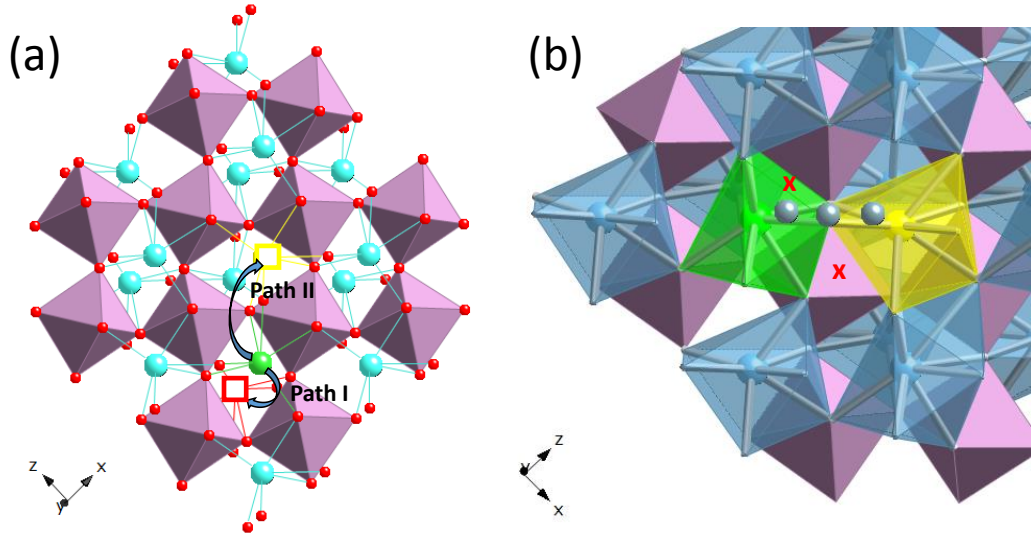

Figure 4.- (a) The two investigated paths for Ca diffusion in $CaMoO_3$. Color code: Mo in pink, Ca in blue with the diffusing Ca^{2+} in green and the vacant sites in red and yellow. (b) Ca motion along path II. Red crosses indicate the common face between the Ca-Ca intersites and Mo polihedra.

Figure 5 shows the calculated energy barriers for path I and II in the $Ca_{15}Mo_{16}O_{48}$ supercell. In both cases, the Ca mobility is hindered, with barriers exceeding 2 eV. Larger supercells have been considered to minimize the interaction between defects. Hence, for path I we have also calculated the barrier in a $Ca_{31}Mo_{32}O_{96}$ supercell with a = 11.2 Å, b= 15.6 Å and c= 10.9 Å. It can be seen in **figure 5** that the calculated barrier is above 2 eV. The analysis of the crystal structures suggests that the high motion barrier is due to the impossibility of Ca ions to occupy the closer vacant site (denoted by red crosses in **figure 4b**) since a Ca diffusing ion in this site would share a face with the octahedron coordinating Mo. To avoid this electrostatic repulsion, the diffusing Ca ion must pass across the shared edge with the neighbour Ca site (grey balls in **figure 4b**). The Ca-O distance is then too short, 2.11 Å, prohibiting the mobility of the Ca^{2+} ion. Therefore, the low mobility of Ca ions seems to be intrinsic to the perovskite crystal structure, and no compositional modifications would diminish the barrier.

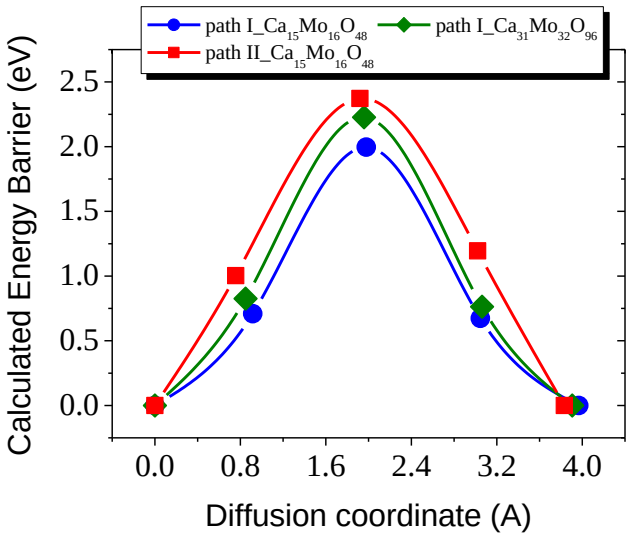

Figure 5.- Calculated energy barrier for Ca diffusion in $CaMoO_3$. Path I and II are shown in figure 4.

Following the computational research, an experimental investigation of the material is critical to conclude whether Ca ions can be extracted from $CaMoO_3$. The synthesis procedure of $CaMoO_3$ requires a reduction step from the $CaMoO_4$ precursors (see methodology section), and, unsurprisingly, if overreduction occurs metallic molybdenum is formed. Determining the precise time and atmosphere of the reduction process is difficult, as pointed out by other authors [37]. In the present work optimization of the reduction process leads to an almost pure phase with a reduced molybdenum metal content of 2.5% (small peak at 40.58°). **Figure 6** shows the XRD pattern with Rietveld fit. The refined lattice parameters for $CaMoO_3$ (5.45132 Å, 5.58613 Å and 7.78321Å) are in good agreement with previous reports [15], [37]. The Bragg R factor for the $CaMoO_3$ phase is calculated to 3.97.

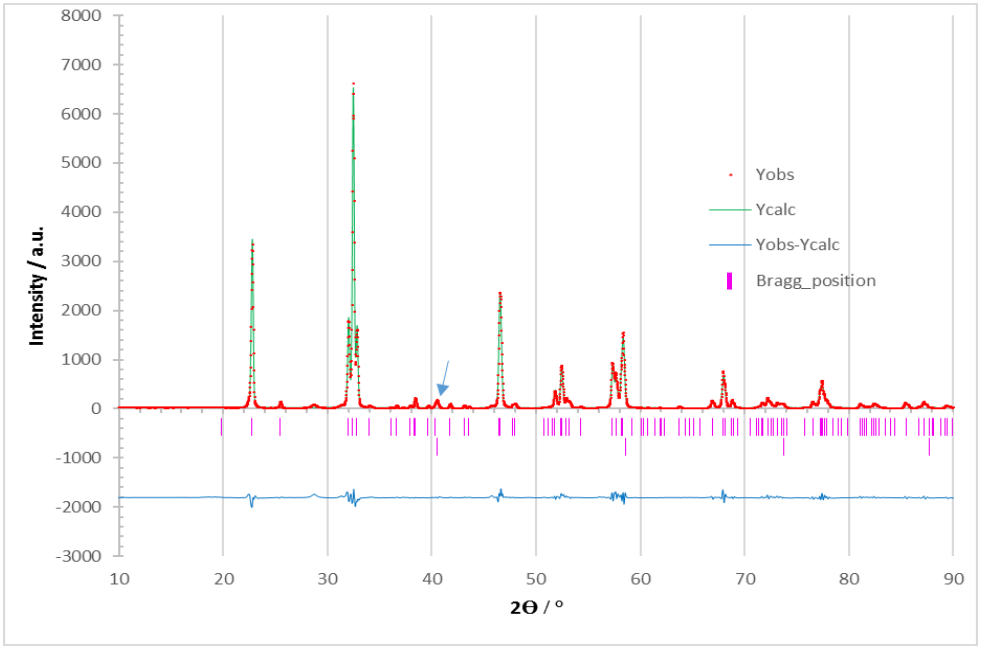

Figure 6. XRD and Rietveld analysis of $CaMoO_3$ (prepared by Ar/H_2 treatment of commercial $CaMoO_4$).

$Ca//CaMoO_3$ cells were tested under different protocols. The expected theoretical capacity for a full deinsertion of Ca^{2+} is 291mAh/g. **Figure 7** shows the oxidation of a $CaMoO_3$ casted electrode charged by PITT using a 5mV step and a cut off current of C/200 at 50°C. No significant electrochemical capacity is achieved until the potential reaches high values and a long plateau is observed at ca. 4.2 V. This plateau is indicative of the electrolyte degradation, in agreement with the XRD pattern of electrodes before and after oxidation which do not exhibit any difference (not shown for conciseness). Similar results were obtained independently of the electrochemical protocol (PITT, GCPL) chosen and temperature (50 -75 ºC) applied and no signature of electrochemical activity due to the Ca deinsertion from the active material could be achieved, which, in view of the above described results, can be attributed to the low ionic mobility.

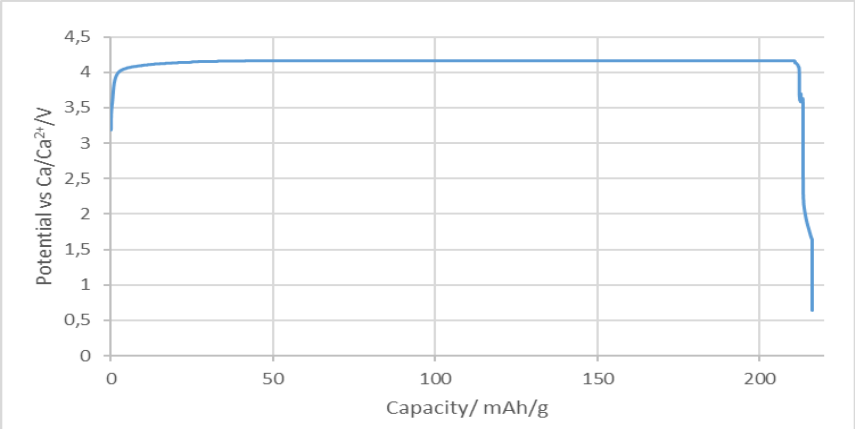

Figure 7.- PITT charge curve of a $CaMoO_3$ coated electrode by applying 5mV steps and a cut off current of C/200 at 50°C.

Conclusions

First principles calculations allow predicting basic electrochemical characteristics of $CaMO_3$ perovskites considered as cathode materials for Ca ion batteries. Full or partial Ca deinsertion from orthorhombic $CaMO_3$ perovskites (M = Cr, Mn, Fe, Co, Ni) would occur at voltages above 3.5 V and be associated to important crystal structure modifications (irreversible reactions). $CaMoO_3$ is identified as the most interesting material, which combines good electronic conductivity, moderate crystal structure modifications, activity in the 2-3 V region, and several intermediate Ca_xMoO_3 stable phases. However, the calculated barriers for Ca^{2+} motion in $CaMoO_3$ are above 2 eV. In agreement with that trend, none of the experimental attempts using different conditions (C/rate, temperatures) did allow to detect Ca deinsertion from $CaMoO_3$. Based on the DFT results, this lack of electrochemical activity is ascribed to the low Ca diffusion in the perovskite structure. We expect that the capability of Ca_xMoO_3 to undergo redox reactions in the range $0 < x < 1$ at a 2.5-3 V and with moderate volume

variations would be retained in other structural types and thus investigation of Mo compounds crystallizing in other structures with more favourable paths for Ca diffusion are underway.

This work highlights the usefulness of using DFT results as a guiding tool in the development of cathodes for multivalent based batteries. Indeed, even for crystal chemistry intercalation favoured structures, the large charge to radius ratio can be an issue and thus multivalent ion diffusion is a crucial parameter to consider. DFT can thus serve to accelerate the screening of potentially interesting positive electrode materials saving experimental time and allowing to assess the validity of the experimental results which could be biased by existing issues related to electrolyte compatibility or negative electrode reliability in these technologies, currently under development at all levels.

Acknowledgments: Authors would like to thank F. Rosciano for advice and support in synthesizing the perovskite material and A. Ponrouch and D. Tchitchekova for assistance with the electrochemical tests. The Toyota Battery Research division at Higashi Fuji (M6) is acknowledged for financial support and ICMAB authors are grateful to the Spanish Ministry of Economy and Competitiveness for support through "Severo Ochoa" Programme for Centres of Excellence in R&D (SEV- 2015-0496)..

References

1. J. Muldoon, C. B. Bucur and T. Gregory, *Chem. Rev*, 2014, **114**, 11683.
2. A. Ponrouch, C. Frontera, F. Barde and M. R. Palacin, *Nature Materials*, 2015, **DOI:10.1038/NMAT4461**.
3. M. Hayashi, H. Arai, H. Ohtsuka and Y. Sakurai, *Electrochemical and Solid State Letters*, 2004, **7**, A119.
4. G. G. Amatucci, F. Badway, A. Singhal, B. Beaudoin, G. Skandan, T. Bowmer, I. Plitza, N. Pereira, T. Chapman and R. Jaworski, *Journal of the Electrochemical Society*, 2001, **148**, A940.
5. J. Rogosic, *"Towards the Development of Calcium Ion Batteries"* Massachussets Institute of Technology, Thesis Advisor; D. Sadoway, 2014.
6. A. L. Lipson, B. Pan, S. H. Lapidus, C. Liao, J. Y. Vaughey and B. J. Ingram, *Chem. Mater*, 2015, **27**, 8442.
7. Y. S. Meng and M. E. Arroyo-de Dompablo, *Energy and Environ. Science*, 2009, **2**, 589.
8. T. Zhang, D. Li, Z. Tao and J. Chen, *Progress in Natural Science-Materials International*, 2013, **23**, 256.
9. Y. L-M., S. J-M., C. Sun and B.-H. Yue, *Advances in Manufacturing*, 2014, **2**, 358.
10. G. Ceder, *Mater. Res. Soc. Bull.*, 2010, **35**, 693.
11. M. S. Islam and C. A. J. Fisher, *J. Chem. Soc. Rev.*, 2014, **43**, 185.
12. M. Liu, Z. Rong, R. Malik, P. Canepa, A. Jain, G. Ceder and K. A. Persson, *Energy & Environmental Science*, **8**, 964.
13. R. D. Shannon and C. T. Prewitt, *Acta Crystallographica*, 1976, **32**, 751.
14. D. Er, J. Li, M. Naguib, Y. Gogotsi and V. B. Shenoy, *Acs Applied Materials & Interfaces*, **6**, 11173.

15. C. de la Calle, J. A. Alonso, M. Garcia-Hernandez and V. Pomjakushin, *Journal of Solid State Chemistry*, 2006, **179**, 1636.
16. A. M. Arevalo-Lopez, B. Liang, M. S. Senn, C. Murray, C. Tang and J. P. Attfield, *Journal of Materials Chemistry C*, 2014, **2**, 9364.
17. K. R. Poeppelmeier, M. E. Leonowicz, J. C. Scanlon, J. M. Longo and W. B. Yelon, *Journal of Solid State Chemistry*, 1982, **45**, 71.
18. T. Takeda, R. Kanno, Y. Kawamoto, M. Takano, S. Kawasaki, T. Kamiyama and F. Izumi, *Solid State Sciences*, 2000, **2**, 673.
19. G. Kresse and J. Furthmuller, *Physical Review B*, 1996, **54**, 11169.
20. J. P. Perdew, K. Burke and M. Ernzerhof, *Physical Review Letters*, 1996, **77**, 3865.
21. P. E. Bloch, *Phys. Rev. B*, 1994, **50**, 17953.
22. P. Erhart, A. Klein, D. Aberg and B. Sadigh, *Physical Review B*, 2014, **90**.
23. N. Hamdad and B. Bouhafs, *Physica B-Condensed Matter*, 2010, **405**, 4595.
24. J. Hong, A. Stroppa, J. Iniguez, S. Picozzi and D. Vanderbilt, *Physical Review B*, **85**.
25. J. Hong, A. Stroppa, J. Iniguez, S. Picozzi and D. Vanderbilt, *Physical Review B*, 2012, **85**.
26. S. F. Matar, *Progress in Solid State Chemistry*, 2003, **31**, 239.
27. Y. Wang, S. H. Lee, L. A. Zhang, S. L. Shang, L. Q. Chen, A. Derecskei-Kovacs and Z. K. Liu, *Chemical Physics Letters*, **607**, 81.
28. A. C. Komarek, S. V. Streltsov, M. Isobe, T. Möller, M. Hoelzel, A. Senyshyn, D. Trots, M. T. Fernández-Díaz, T. Hansen, H. Gotou, T. Yagi, Y. Ueda, V. I. Anisimov, M. Grüninger, D. I. Khomskii and M. Braden, *Phys. Rev. Lett.*, 2008, **101**, 167204.
29. M. S. Islam, *J. Mater. Chem.*, 2000, **10**.
30. H. M. Liu, C. Zhu, C. Y. Ma, S. Dong and J. M. Liu, *Journal of Applied Physics*, 2011, **110**.
31. J. B. Yang, M. S. Kim, Q. Cai, X. D. Zhou, H. U. Anderson, W. J. James and W. B. Yelon, *Journal of Applied Physics*, 2005, **97**.
32. S. L. Dudarev, G. A. Botton, S. Y. Savrasov, Z. Szotek, W. M. Temmerman and A. P. Sutton, *Physica Status Solidi a-Applied Research*, 1998, **166**, 429.
33. C. Frontera and J. Rodriguez-Carvajal, *Physica B-Condensed Matter*, 2004, **350**, E731.
34. E. Castillo-Martinez, A. Duran and M. A. Alario-Franco, *Journal of Solid State Chemistry*, 2008, **181**, 895.
35. M. E. Spahr, P. Novák, O. Haas and R. Nesper, 1995, **54**, 346.
36. K. Kamata, T. Nakamura and T. Sata, *Chemistry Letters*, 1975, DOI: 10.1246/cl.1975.81, 81.
37. H. N. Im, S. Y. Jeon, M. B. Choi, H. S. Kim and S. J. Song, *Ceramics International*, **38**, 153.

Supplementary Information

TABLE I: Theoretical specific capacity (in mAh/g-$CaMO_3$) of some of the investigated $CaMO_3$ perovskites assuming 100% calcium de-intercalation

TM	Mo	Cr	Mn	Fe	Co	Ni
Theoretical specific capacities (mAh/g)	291	383	375	372	364	365

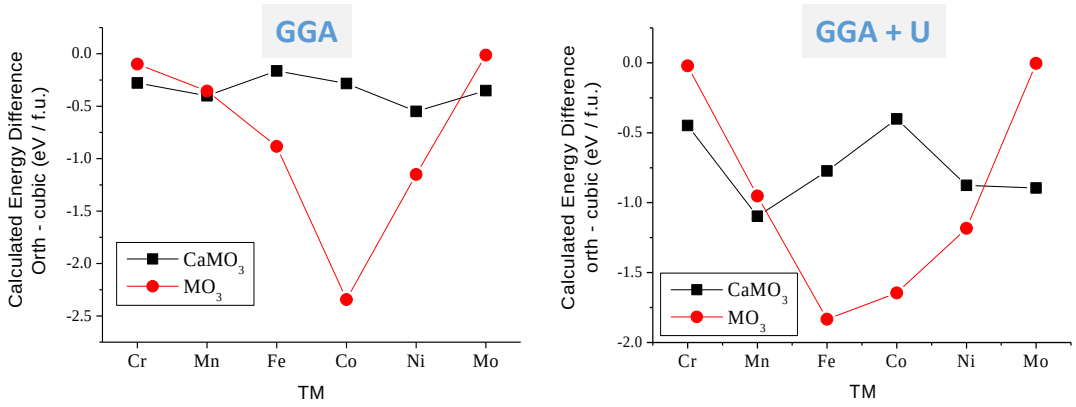

Figure 1.- Calculated energy difference between the cubic and the orthorhombic symmetry for $CaMO_3$ (black squares) and MO_3 (red circles) perovskites within the GGA approximation (left) and the GGA+U (right).

TABLE II. Calculated lattice parameters (in Å) for orthorhombic MO_3 structures (S.G. *Pnma*) within the GGA and the GGA+U method.

TM	Approximant	*a*	*b*	*c*
Mo	GGA	5.383	7.539	5.283
	GGA+U	5.388	7.547	5.289
Cr	GGA	4.940	6.938	4.823
	GGA+U	4.493	6.943	4.825
Mn	GGA	4.839	6.802	4.695
	GGA+U	4.831	6.909	4.766
Fe	GGA	5.356	6.015	4.720
	GGA+U	5.625	6.211	5.165
Co	GGA	4.578	6.878	4.604
	GGA+U	4.834	6.957	4.881
Ni	GGA	4.753	6.732	4.704
	GGA+U	4.728	6.741	4.673

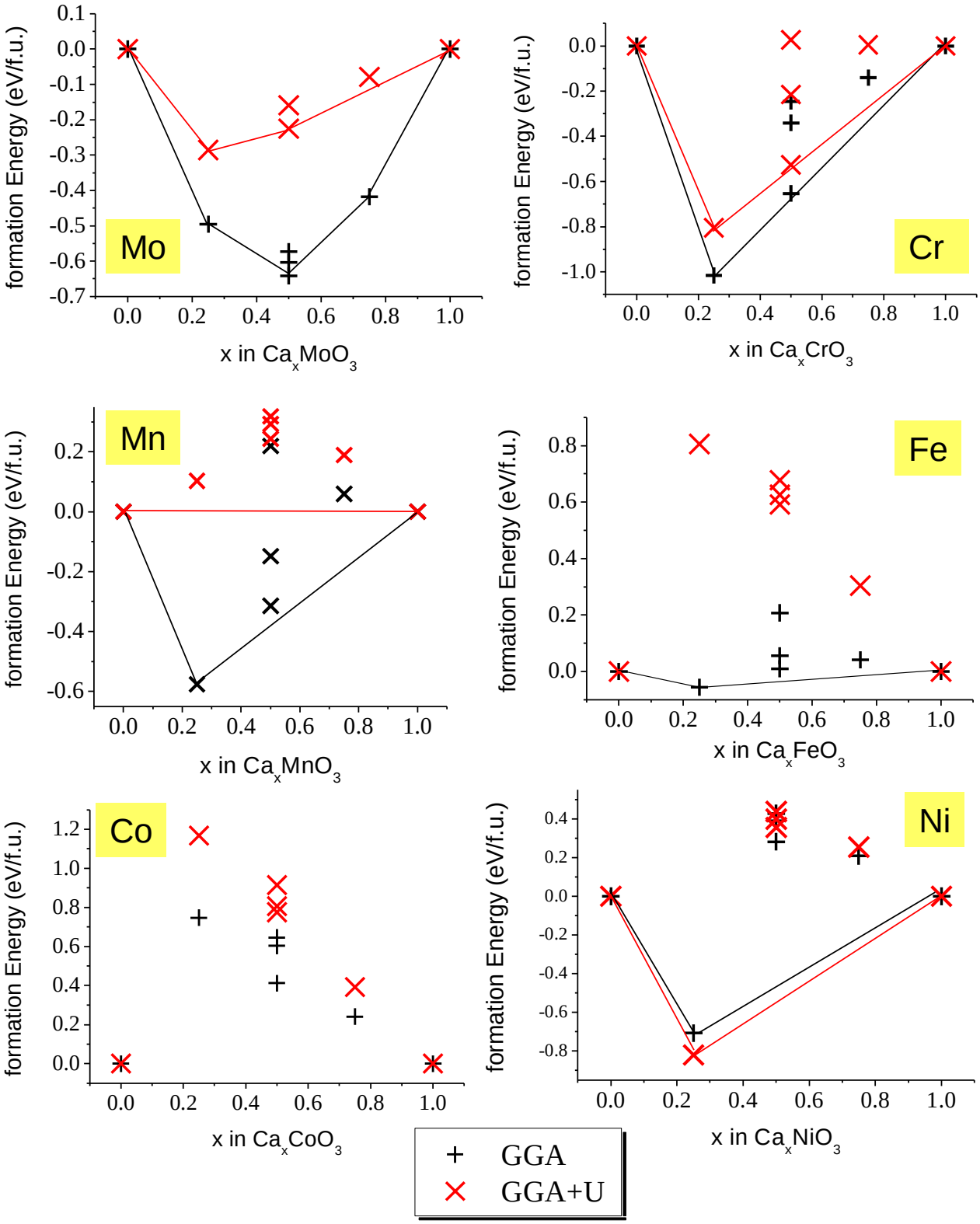

Figure 2.- Calculated formation energies of ordered Ca_xMO_3 structures as a function of the calcium concentration. Red for GGA+U and black for GGA.